


# $[^{11}\text{C}]$ acetate and PET/CT assessment of muscle activation in rat studies

Sara Trombella<sup>1</sup>  · David García<sup>1</sup> · Didier J. Colin<sup>2</sup> · Stéphane Germain<sup>2</sup> · Yann Seimbille<sup>3</sup> · Osman Ratib<sup>3</sup>

Received: 12 January 2015 / Accepted: 2 July 2015 / Published online: 26 July 2015  
© CARS 2015

## Abstract

**Purpose** The purpose of the present study is to apply kinetic analysis to investigate exercise-related changes in the metabolism of the skeletal muscle of the rat hindlimb by  $[^{11}\text{C}]$ acetate positron emission tomography and computed tomography (PET/CT).

**Methods** Contractions were induced in Wistar rats' left hindlimb by electrostimulation of the Vastus Lateralis muscle motor point. After 15 min of muscle contractions,  $[^{11}\text{C}]$ acetate was injected and PET/CT of both hindlimbs was acquired. The resting hindlimb was used as a control reference. The kinetic parameters  $K_1$  and  $k_2$  were calculated for the target muscles (exercised and control) and correlated with the corresponding standardized uptake values (SUVs). The ratio between each kinetic parameter values and the SUV

extracted for the exercised muscle and the muscle at rest was computed ( $K_1^{Ex}/K_1^{Re}$ ,  $k_2^{Ex}/k_2^{Re}$  and  $\text{SUV}^{Ex}/\text{SUV}^{Re}$ , respectively).

**Results** Kinetic analysis quantitatively confirmed that net tracer uptake ( $K_1$ ) and washout ( $k_2$ ) were significantly higher in exercised muscles ( $K_1$  :  $0.34 \pm 0.12 \text{ min}^{-1}$  for exercised muscles vs.  $0.18 \pm 0.09 \text{ min}^{-1}$  for resting muscles,  $P = 0.01$ ;  $k_2$  :  $0.22 \pm 0.05 \text{ min}^{-1}$  for exercised muscle vs.  $0.14 \pm 0.04 \text{ min}^{-1}$  for resting muscle,  $P = 0.002$ ). On the other hand, SUV was not significantly different between active and inactive muscles ( $0.7 \pm 0.2$  for exercised muscles vs.  $0.6 \pm 0.1$  for resting muscles). Linear regression analysis revealed a good correlation ( $R^2 = 0.75$ ,  $P = 0.005$ ) between net tracer uptake ratio ( $K_1^{Ex}/K_1^{Re}$ ) and the SUV ratio ( $\text{SUV}^{Ex}/\text{SUV}^{Re}$ ). A lower correlation was found between the net tracer washout ratio ( $k_2^{Ex}/k_2^{Re}$ ) and the SUV ratio ( $R^2 = 0.37$ ,  $P = 0.1$ ).

**Conclusion** The present study showed that kinetic modelling can detect changes between active and inactive skeletal muscles with a higher sensitivity with respect to the SUV, when performed with  $[^{11}\text{C}]$ acetate PET/CT.

**Keywords**  $[^{11}\text{C}]$ acetate · PET/CT · SUV · Kinetic analysis · Muscle contraction

✉ Sara Trombella  
Sara.Trombella@hcuge.ch

David García  
David.Garcia@hcuge.ch

Didier J. Colin  
Didier.Colin@hcuge.ch

Stéphane Germain  
Stephane.Germain@hcuge.ch

Yann Seimbille  
Yann.Seimbille@hcuge.ch

Osman Ratib  
Osman.Ratib@hcuge.ch

<sup>1</sup> University of Geneva and University Hospitals of Geneva, 4 Rue Gabrielle-Perret-Gentil, 1211 Geneva 14, Switzerland

<sup>2</sup> University Hospitals of Geneva and Centre for Biomedical Imaging (CIBM), 4 Rue Gabrielle-Perret-Gentil, 1211 Geneva 14, Switzerland

<sup>3</sup> University Hospitals of Geneva, 4 Rue Gabrielle-Perret-Gentil, 1211 Geneva 14, Switzerland

## Introduction

PET imaging, using specific radiopharmaceuticals, provides quantitative radioactivity measurements within a target body region or organ. This can allow for a better understanding of biochemical and metabolic processes, as well as answer several clinical questions about organ function and diseases. Tracer kinetic modelling techniques can improve the quality of information inferred from these biological data.

Nowadays, kinetic models represent well-established methods for quantification of regional metabolic processes in vivo. An advantage, when using hybrid PET/CT, is the possibility of combining functional PET images with anatomic information from CT images, ensuring a precise location of the target tissue.

[ $^{11}\text{C}$ ]acetate has been extensively used as a tracer in staging primary and recurrent prostate cancer with PET [25,32,37,43].

In cardiac studies, [ $^{11}\text{C}$ ]acetate has been used for evaluating myocardial oxygen consumption ( $\text{MVO}_2$ ) and myocardial blood flow (MBF): in particular, this specific tracer has been validated for myocardium in animal [1,2,5,8] and human [17,40] studies to evaluate these two indexes as relevant measures to understand various physiological pathways and diseases. Ng et al. [31] and van den Hoff et al. [15] proposed six- and five-tissue compartment models, respectively, to model myocardial [ $^{11}\text{C}$ ]acetate kinetics. Such models offer a detailed description of [ $^{11}\text{C}$ ]acetate kinetic paths within the myocardium. However, high complexity make these models impractical and error prone when applied to PET images. Simpler one- and two-tissue compartment models were validated by Sun et al. [39] and Buck et al. [5] in myocardium, and later applied to prostate oncology by Schiepers et al. [37].

Van Hall et al. [13] studied human whole-body and leg [ $^{13}\text{C}$ ] acetate kinetic at rest, during exercise and recovery. In this study, the authors conclude that inactive skeletal muscle plays a minor role in acetate turnover, whereas active skeletal muscle enhances several-fold acetate uptake and subsequent oxidation, as well as release and contribution to whole-body acetate turnover. Buchegger et al. [4], within their study of muscle function after hip arthroplasty with [ $^{11}\text{C}$ ]acetate PET/CT, visualized a consistent increase in [ $^{11}\text{C}$ ]acetate uptake in healthy muscles under exercise compared with muscles at rest, and measured mean standardized uptake values (SUVs) within regions of interest (ROIs) drawn over individual muscles. Croteau et al. [9] applied a two-tissue compartment model, previously validated in myocardium, to evaluate the perfusion index of human skeletal muscle at rest with PET/CT images.

Our present study is part of a larger European Marie-Curie project (Multiscale Biological Modalities for Physiological Human Articulation [29]), whose final goal will be the development of visualization/interaction tools to allow a better assessment of musculoskeletal systems in motion and a structural and functional comprehension of the human body, merging several data types of different scales, acquired from different imaging modalities.

In the present study, we aim to apply kinetic analysis to investigate [ $^{11}\text{C}$ ]acetate uptake in the rat hindlimb skeletal muscle by PET/CT, in view of the development of a model applicable in humans for in vivo quantitative assessment of muscular activity. With respect to previous works concerning

the study of the muscle by [ $^{11}\text{C}$ ]acetate kinetic [5,9,13], we apply here a one-tissue compartment model to investigate the differences in acetate uptake between the exercised and resting skeletal muscles of the rat. The advantage of the SUV is its computational simplicity that in part is responsible for its extensive usage in the daily clinical practice. Despite its popularity, its accuracy and reproducibility are still controversial [18], since it only provides an estimated measure of the real tracer uptake within a tissue at a particular time relative to tracer injection. A model approach requires as input data the concentration activity in the arterial blood and in the target tissue as a function of time, respectively known as input function (IF) and tissue time-activity curve (TAC). However, the higher complexity of kinetic modeling methods should be weighted against their capability to account for the physiological and biological time course of the tracer activity within the blood and tissues. It is important to underline that kinetic analysis provides complimentary information to the SUV. Our goal is to evaluate to which extent kinetic rate constants obtained from a one-compartment kinetic model can better distinguish between exercised and resting muscles, and how these parameters correlate with the SUVs computed over the same regions.

### [ $^{11}\text{C}$ ]acetate kinetic modelling

Almost all aerobic organisms carry out a metabolic path known as oxidative phosphorylation in order to produce adenosine triphosphate (ATP). This molecule is used in cells as a coenzyme and is responsible for supplying energy to metabolism. Acetate, a free fatty acid (FFA), enters the TCA cycle directly after conversion to acetyl-CoA; thus, it can be used to measure the flux of the TCA cycle and the production of reducing equivalents. As this is coupled to oxygen consumption, the latter can be estimated by measuring the flux through the TCA cycle with acetate.

It was demonstrated in cardiac studies that accurate noninvasive simultaneous estimations of absolute  $\text{MVO}_2$  and MBF are possible with [ $^{11}\text{C}$ ]acetate and a simple compartment model using PET [5,39]. Tissue [ $^{11}\text{C}$ ] clearance kinetics can be adequately described also by mono-exponential or bi-exponential functions. The advantage of the exponential fitting approach is its simplicity. However, although the exponential curve fitting method for determining rate constants of oxidative metabolism has proven useful, the model approach offers many advantages.

Sun et al. [39] demonstrated that a simplified two-compartment model for [ $^{11}\text{C}$ ]acetate can be used to simultaneously derive accurate estimates of absolute  $\text{MVO}_2$  and MBF in a noninvasive way. As reported by the authors, mono-exponential fitting of the myocardial TAC can significantly be affected by the shape of the arterial IF and be misinterpreted as true changes in the  $\text{MVO}_2$ . Furthermore,

mono-exponential curve fitting method is more subjective than a compartment model approach, as it relies on the correct selection of the data points on the TAC. Bi-exponential fit also requires more subjective selection of the time interval for fitting that could show an interstudy variability. A model approach potentially yields absolute values of regional  $\text{MVO}_2$ , rather than only indices of oxidative metabolism. Moreover, a compartment model accounts for those changes in the IF that can be due to several biological factors, e.g. the rate of tracer injection, cardiac chamber volumes and/or cardiac output. The IF can also be incorporated into the bi-exponential model by convolution with the exponential function. However, the computational drawback of such procedure is that the fit will not be linear in the semilogarithmic domain anymore, thus losing its simplicity.

Buck et al. [5] highlighted another advantage of kinetic models versus exponential fitting techniques. As described in their work, these models do not take into account recirculating [ $^{11}\text{C}$ ]acetate activity in blood. The authors prove that the correlation coefficient between clearance rate and rate-pressure product for a one-tissue model is substantially higher than the correlation determined by mono-exponential fitting, most likely due to the ability of the model approach to account for recirculating [ $^{11}\text{C}$ ]acetate occurring after intravenous injection of the tracer, by introducing a correction for labelled metabolites in blood. The final results of the study suggest that the noninvasive estimation of myocardial oxygen consumption in human subjects by [ $^{11}\text{C}$ ]acetate PET imaging can be improved by use of a compartmental model.

## Materials and methods

### Animals

All animal preparation procedures and experiments were performed in accordance with local and federal guidelines and were approved by the local veterinary ethics committee from the canton Geneva. Eight male healthy Wistar rats were initially obtained at 7 weeks of age from Charles River Laboratories (L'Abresle Cedex, France). Average (AV)  $\pm$  standard deviation (SD) body weight at testing was  $372 \pm 25$  g.

### Animal preparation

The animals were housed under standard 12:12-h light/dark conditions, with free access to food and water. Each animal was placed first inside an induction chamber with 1–5% isoflurane and 1L/min oxygen until it became unconscious. After this initial induction (45–60 s), the animal was placed on a warm surgery plate and nose-coned to gas anaesthesia

(1–5% isoflurane in 1L/min oxygen) during subsequent microsurgical procedures and imaging sessions. All equipment are commercially available (surgery equipment: Harvard Apparatus, Holliston, MA, USA; anaesthesia equipment: Minerve, 51310 Esternay, France). Clean microsurgery was performed for arterial and venous catheter placement. The insertion of stable and secure vascular catheters is necessary to allow radiotracer injection and input function (IF) extraction through an external arteriovenous loop during PET imaging. The jugular vein and the carotid artery were chosen due to ease of access and size of vessel. This kind of surgery was preferred to the femoral arteriovenous loop because located outside the imaging FOV in this study. A Leica binocular microscope (6 $\times$  magnification) was used to perform the microsurgery and catheter placement. The neck area was shaved and cleansed with alcohol scrubs to establish a clean field. A small surgical incision was made in the appropriate anatomical area (jugular vein, carotid artery), and tissue surrounding the blood vessel was gently dissected using appropriate surgery equipment. Polyethylene catheters PE50 (0.58 mm internal diameter; 0.965 mm outer diameter), prefilled with 420 U/mL heparinized saline, were used for vessel catheterization. The left carotid artery was cannulated for the measurement of the arterial IF with an external microvolumetric  $\beta$  blood counter ( $\mu\text{BC}$ ) [6]. The left jugular vein completed the arteriovenous shunt, guided through the  $\mu\text{BC}$ . The tail vein was cannulated with an intravenous (IV) catheter (BD Insyte-W 24GA) to allow for tracer injection (Fig. 1). After surgery, the animal was placed prone on the heated PET bed of the scanner, and anaesthesia was maintained with 1–3.5% isoflurane in 1 L/min oxygen. In this specific experimental and surgical set-up, a lower percentage than 1% would have represented a risk for the anaesthesia not to be effective during the whole procedure. On the other hand, a higher percentage than 3.5% could have determined the death of the animal for stroke or other complications. Conventional monitoring devices were used in association with the PET/CT scanner.

### Stimulation procedure

Electrostimulation was delivered to the animal subject in order to induce physiological contractions of the VL muscle (knee extensor) and to simulate voluntary repeated extensions of the knee joint. Under aseptic conditions, mono-polar needle electrodes were inserted into the VL muscle of the left hindlimb for motor point stimulation, and kept in place by mean of a laboratory support. The choice of the muscle was guided by its contribution to knee movement and by its relatively wide extension within the upper hindlimb of the animal. The anatomy of muscle motor points within the rat hindlimb is well known from the literature [23]. A pulse generator (FHC Pulsar 6dp Stimulator, FHC Inc.) was

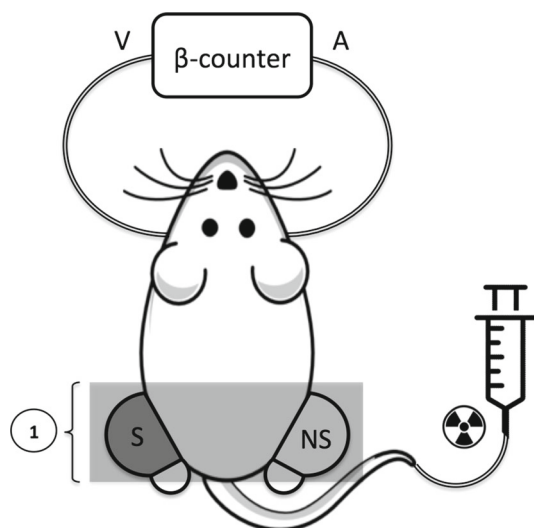


**Fig. 1** Experimental set-up: the left carotid artery was catheterized for the measurement of the arterial IF with an external  $\mu$ BC. The left jugular vein was cannulated to complete the arteriovenous shunt. [ $^{11}\text{C}$ ]acetate was injected in the lateral tail vein. (I) The PET FOV was centred over the upper part of the hindlimbs. Both target muscles, stimulated (S) and not (NS), as well as the IVC, were imaged within the FOV

used to deliver the electrical stimulation. For each experiment, the motor point was identified as the point of greatest contraction after percutaneous stimulation of the target muscle using a low current. Muscle stimulation was delivered as cyclic trains of electrically isolated biphasic current pulses provided to the target muscle. Biphasic pulses were preferred for chronic electrical muscle stimulation to prevent net ion flow that could result in tissue damage or electrode corrosion [34].

Three stimulation protocols were tested, as detailed in Table 1. In a first group of rats ( $N = 6$ ), a decrease in joint angular excursion was observed after the first minutes of stimulation. In some cases, this decrease continued until a

complete stop. In such cases, it was possible to restore the movement by adjusting electrode position within the muscle. However, joint angular excursion was typically lower after subsequent electrode repositioning. In a single experiment ( $N = 1$ ), the current amplitude was progressively increased, as the knee angular excursion got feeble. This allowed maintaining a nearly constant knee angular excursion during the whole stimulation protocol. Still, it was necessary to adjust the electrode position within the muscle during the experience. In a single experiment ( $N = 1$ ), pulse frequency was set to 7.5 kHz [23], and current amplitude was progressively increased in order to maintain a nearly constant knee angular excursion. Also in this case, it was necessary to adjust electrode position within the muscle during the experience. The size of the stimulated hindlimb did not change in a sensible way with respect to the inactive one.

Immediately after the stimulation procedure, the animal was moved to the PET scanner for imaging.

## Data acquisition

### PET/CT image acquisition and processing

PET and CT images were acquired on a FLEX Triumph PET/SPECT/CT scanner (Gamma Medica Inc./TriFoil) [35]. PET data were acquired first. Immediately after, a CT scan was performed for anatomical purpose.

PET study emission data were recorded in list mode for a total time of 40 min and reconstructed dynamically using the three-dimensional ordered-subset expectation maximization (OSEM 3D) algorithm. The dynamic PET frame sequence was chosen to be:  $12 \times 15$  s,  $8 \times 30$  s,  $3 \times 60$  s and  $6 \times 300$  s frames [9]. The reconstructed standard in-slice pixel size was 0.5 mm, and the slice thickness was 0.597 mm. For the scanner used in this study, PET radial full width at half maximum (FWHM) varies between 2.0 mm in the centre of

**Table 1** Three stimulation protocols were tested. In a first group of rats ( $N = 6$ ), the amplitude of the stimulation current was set to  $1.5 \times$  the threshold current (TC) known to produce visual twitches (lowest current

needed to obtain a smooth muscle contraction [22] at the  $40 \mu\text{s}$ /phase pulse width), at a pulse width of  $40 \mu\text{s}$  and a frequency of 75 Hz

N	Pulse frequency (Hz)	Current amplitude (mA)	Pulse width ( $\mu\text{s}$ )	Stimulus burst duration (ms)	Stimulus cycle (ms)	Stimulus duration (min)
6	75	$1.5 \times TC$	40	240	500	15
1	75	$1.5 \times TC$ to 4	40	240	500	15
1	7.5k	$1.5 \times TC$ to 2.5	40	240	500	15

Stimulations were performed every 0.5 s for 15 min, while the rat was anesthetized, as reported by Jung et al. [22] and Kanchiku et al. [23]. As reported by Thota et al., the neural activity in the flexor and extensor muscles in rat joints occurs in bursts and has a typical relationship to the stance and swing phases of the normalized gait cycle. The mean burst duration of the VL muscle during stance was reported to be  $221.7 \pm 19.4$  ms [42]. In accordance with this study, pulse duration was set to 240 ms, with the purpose to simulate a locomotor-type movement of the muscle by electrostimulation. According to Kanchiku et al. [23], to reach this goal, it is necessary to obtain sufficient angular excursion of the involved joint during electrically induced movements. In a single experiment, the current amplitude was progressively increased from  $1.5 \times TC$  to 4 mA, as the knee angular excursion got feeble. In the last experiment, pulse frequency was set to 7.5 kHz [23], and current amplitude was progressively increased from  $1.5 \times TC$  to 2.5 mA



the field of view (CFOV) and 2.3 mm at a radial offset of 25 mm, whereas the axial FWHM ranges between 2.8 and 3.2 mm for the same radial offset [35]. The animals were placed prone, head first on the experimental bed. The field of view (FOV) was centred on the upper part of the lower limbs. Both hindlimbs were imaged within the FOV. Within 10 s from data acquisition start, the animal received a bolus injection of  $43 \pm 6$  MBq of [ $^{11}\text{C}$ ]acetate, followed by a saline chase. The FLEX Triumph built-in calibration method was used to obtain quantified images in Bq/mL. No scatter and attenuation correction were applied.

To acquire CT images, the X-ray tube was set at 80 kVp and tube current of  $160 \mu\text{A}$ . A total of 1024 projections were acquired during the  $360^\circ$  rotation. The Triumph XO software, which uses a back-projection engine, was used to reconstruct the CT scans with a in-slice voxel matrix of  $512 \times 512$  voxels, isotropic voxel size of 0.17 mm and a circular field of view of 92.16 mm. Reconstructed CTs were co-registered with the PET scans using the plugin Vivid (Gamma Medica / Trifoil) for Amira (FEI) and exported as DICOM files for high-resolution visualization of the rats' anatomy. Voxel-by-voxel analyses were allowed by resampling the CT scans according to the resolution of the PET scans with Amira. The dimension of the CT data set was first adjusted according to the dimension of the PET data set ( $100 \times 100 \times 76.38$  mm). The CT data set was then resampled according to the OSEM 3D resolution ( $200 \times 200 \times 128$ ) and voxel size used to reconstruct the PET scans. Resampled CT data sets were finally stored as DICOM files.

The software for postprocessing of the PET/CT images was written in MATLAB (The MathWorks Inc.).

#### Microvolumetric $\beta$ blood counter

A microvolumetric  $\beta$  blood counter (Gamma Medica Inc.) was used in this study for real-time arterial IF measurement. An arteriovenous shunt was built between the left carotid artery and the left jugular vein, as detailed in section "Animal preparation". The placement of the catheter allowed for a fraction of the blood to flow outside the body through the catheter [26]. The catheter length was chosen to be 107 cm ( $310 \mu\text{L}$  volume) for the first two experiences. For further cases, the catheter length was increased to 133 cm ( $380 \mu\text{L}$  volume). This was found out to be the optimal length to allow the catheter to easily go from the animal, placed inside the PET scanner, to the  $\mu\text{BC}$  located outside the scanner. The length between the sampling point (carotid artery) and the  $\mu\text{BC}$  varied from  $53 \pm 2$  cm to  $66 \pm 2$  cm between the first two experiences and the following cases. Data acquisition from the  $\mu\text{BC}$  was started simultaneously with PET data acquisition start. The arterial IF measured with the  $\mu\text{BC}$  was set to have a temporal resolution of 1 s. Experimental data were corrected for radioactive decay, delay with respect to

the tissue TACs, and for dispersion through the catheter, as detailed in section "Data correction". Blood transit time from the carotid artery to the  $\mu\text{BC}$  was experimentally measured on a set of four rats (weight  $344 \pm 21$  g; loop catheter length 133 cm), and a wide variability was observed.

#### Data correction

To be used as the arterial IF in the kinetic model, the animal measured activity in blood recorded by the  $\mu\text{BC}$  was corrected for detector efficiency, radionuclide decay time, radioactivity dispersion and propagation delay, and system dead time [6]. No corrections for plasma and metabolites were made.

Prior to the experiment, the  $\mu\text{BC}$  was calibrated for noise and detector efficiency. The acquired data were converted to Bq/ $\mu\text{L}$  and decay-corrected to the injection time. Since the  $\mu\text{BC}$  has been shown to be linear up to 160 kBq/ $\mu\text{L}$  with both  $^{18}\text{F}$  and  $^{13}\text{N}$  and such activities are not used in small animal experiments, no correction for dead time was applied.

As reported by Iida et al. [21] and van de Hoff et al. [16], dispersion of tracer concentration in blood can be parametrized as follows:

$$g(t) = C_a(t) \otimes \frac{e^{-t/\tau}}{\tau} \quad (1)$$

A direct consequence of Eq. 1 is:

$$C_a(t) = g(t) + \tau \times (dg/dt) \quad (2)$$

Therefore, it is possible to correct for dispersion and derive the true IF  $C_a(t)$  by deconvolution from the measured IF  $g(t)$ . In this case, the dispersion function is completely specified by the dispersion time constant  $\tau$  (Eq. 1), which has to be defined for each specific experimental set-up. Convert et al. [6] studied radioactivity dispersion inside a catheter. For a PE50 catheter, the dispersion constant  $\tau$  was parametrized as function of withdrawing speed  $v$  and animal-to-detector distance  $d$ :

$$\tau = \left( \text{Span}_V \times e^{-K_V \times v} + \text{Plateau}_V \right) \times \left( 1 - e^{-K_D \times d} \right) \quad (3)$$

In our study,  $d$  was set as half the carotid–jugular catheter length, and  $v$  as the rat heart pumping speed, inferred from blood transit time from the carotid artery to the jugular vein, given the catheter volume.

The measured IF is affected also by the effect of propagation delay between the target tissue and the detector. Delay was taken into account by shifting the timescale of  $g(t)$  in Eq. 2 by the delay time constant  $\Delta$  [16]:



**Fig. 2** 3D visualization with OsiriX [36] of bolus first-pass frame in a dynamic PET set. The IVC is clearly visible in the rat abdomen

$$C_a(t) = g(t + \Delta) + \tau \times (dg/dt)(t + \Delta) \quad (4)$$

Since a wide variability was measured in the blood transit time from the carotid artery to the  $\mu$ BC, the delay time constant  $\Delta$  was defined for each experimental case by aligning the rising points of the tissue TAC and the corrected IF.

An image-derived input function (IDIF) was derived from the inferior vena cava (IVC) located within the field of view, as previously described by Lanz et al. [27]: the time frame corresponding to the bolus first pass (Fig. 2) was selected and a VOI was constructed within the IVC by placing 1-mm square ROIs over 12 successive axial slices. As reported by Lanz et al., the IDIF measured from the IVC is characterized by a sharp peak corresponding to the bolus passage. When compared to the IDIF, the IF measured with the  $\mu$ BC presents a lower maximum. However, shortly after the peak region, the two curves show a coherent shape (Fig. 3). Therefore, it was possible to compute a scaling factor between PET and  $\mu$ BC quantitative data by comparing the tail regions of the IDIF and IF from the  $\mu$ BC.

In order to derive the TACs, a series of ROIs was placed on the region encompassing the VL muscle in successive CT slices. Due to poor CT resolution with respect to the muscular tissue, the ROIs were manually defined over the target region with reference to the femur bone. The ROI series was then exported to the dynamic PET frames, and the tissue TAC was derived for the target muscle. Two TACs were derived from dynamic PET images: one relative to the stimulated hindlimb, and the second one from the control hindlimb, at rest.

Tissue TACs and the IDIF were corrected for radioactive decay, but not for spillover and partial volume effect.

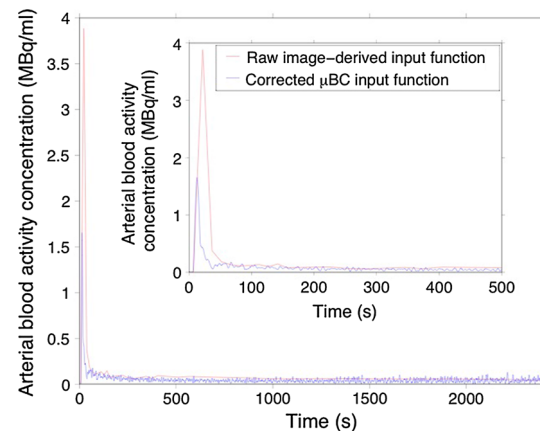


**Fig. 3** Raw IDIF from the IVC (red curve) versus the corrected IF from the  $\mu$ BC (blue curve). The IDIF is characterized by a sharp peak corresponding to the bolus passage. When compared to the IDIF, the IF measured with the  $\mu$ BC reaches a lower maximum. Shortly after the peak region, the two curves show a coherent shape. Inset shows first 500 s of the 2 curves

### Kinetic modelling

For kinetic modelling, the IF was derived from the blood curve measured with the  $\mu$ BC and corrected as detailed in Section “Data correction”. For VL muscle, a one-tissue compartment model (Fig. 4) was used to estimate net tracer uptake,  $K_1$  (mL/g/min) and washout,  $k_2$  ( $\text{min}^{-1}$ ) [3,5]:

$$C_{ROI}(t) = (1 - V_a)K_1C_a(t) \otimes e^{-(K_1/V_d)t} + V_aC_a(t) \quad (5)$$

where  $t$  = time,  $(1 - V_a)$  = perfusable tissue fraction,  $K_1$  = blood flow (or perfusion index),  $C_a(t)$  = activity concentration in arterial blood as function of time,  $V_a$  = arterial blood volume fraction in muscle tissue, and  $V_d$  = volume of distribution of tracer (or partition coefficient),  $k_2 = K_1/V_d$ . By integrating the left- and right-hand sides of Eq. 5, the linear least squares (LLS) solution can be derived, as shown by Feng et al. [11]:

$$C_{ROI}(t) = (1 - V_a) \left[ K_1 \int C_a(t) - (K_1/V_d) \int C_1(t) \right] + V_aC_a(t) \quad (6)$$

using  $C_{ROI} = (1 - V_a)C_1 + V_aC_a$ , where  $C_1$  equals the activity concentration in tissue.

### Statistical analysis

For each animal subject, the kinetic parameters  $K_1$  and  $k_2$  and the average SUV at 20–25 min posttracer administration were obtained independently for the VL muscle in the exercised and resting hindlimbs. The SUV was computed

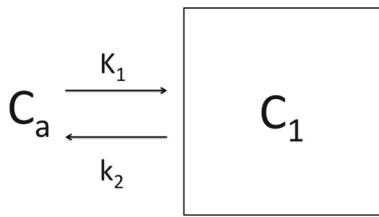


**Fig. 4** One-tissue compartment model:  $C_a(t)$  represents the activity concentration in arterial blood as function of time;  $C_1(t)$  represents the activity concentration in the tissue as function of time;  $K_1$  represents the blood flow (or perfusion index) for tracer moving from the blood to the tissue compartment;  $k_2$  denotes the rate at which the tracer exits the tissue compartment and returns to the blood

on the same VOI defined for the tissue TACs. *t*-testing was used to compare the SUV and kinetic parameters  $K_1$  and  $k_2$  between resting and exercised muscles. The ratios between each kinetic parameter values and the SUV extracted for the active muscle and the muscle at rest were computed ( $K_1^{Ex}/K_1^{Re}$ ,  $k_2^{Ex}/k_2^{Re}$  and  $SUV^{Ex}/SUV^{Re}$ , respectively). The association between each parameter's ratio and the SUV ratio was analysed using linear regression. The results are expressed as  $AV \pm SD$ .

## Results

### Arterial IF correction

An average dispersion constant  $\tau$  of  $11.8 \pm 0.2$  s and an average value of  $20 \pm 13$  s was derived for the delay constant  $\Delta$  over a subset of 4 rats. Since a high variability among time delay constants was observed,  $\Delta$  was derived independently for each experiment, whereas an average  $\tau$  value was assumed for all the experiments. A representative plot of corrected IF and tissue TACs from the exercised and resting muscles is reported in Fig. 5.

The average scaling factor between PET and  $\mu$ BC quantitative data was  $9.6 \pm 1.4$ .

### [ $^{11}\text{C}$ ]acetate tissue uptake

Representative corresponding axial CT and PET images assessing [ $^{11}\text{C}$ ]acetate uptake after muscle contractions are shown in Fig. 6. As clearly visible in the image, uptake of [ $^{11}\text{C}$ ]acetate was significantly higher in the exercised muscle than in the resting muscle.

Linear regression analysis revealed a good correlation ( $R^2 = 0.75$ ,  $P = 0.005$ ) between net tracer uptake ratio ( $K_1^{Ex}/K_1^{Re}$ ) and the SUV ratio ( $SUV^{Ex}/SUV^{Re}$ ). A lower correlation was found between the net tracer washout ratio ( $k_2^{Ex}/k_2^{Re}$ ) and the SUV ratio ( $R^2 = 0.37$ ,  $P = 0.1$ ) (Table 2).

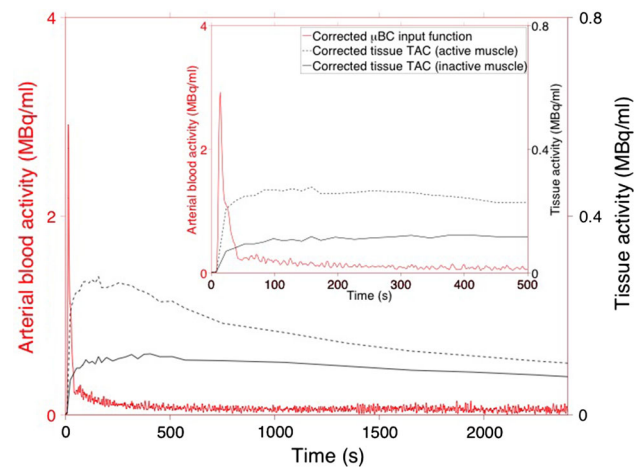


**Fig. 5** Representative corrected IF and tissue TACs for exercised and resting target muscles. *Inset* shows first 500s of the 3 curves

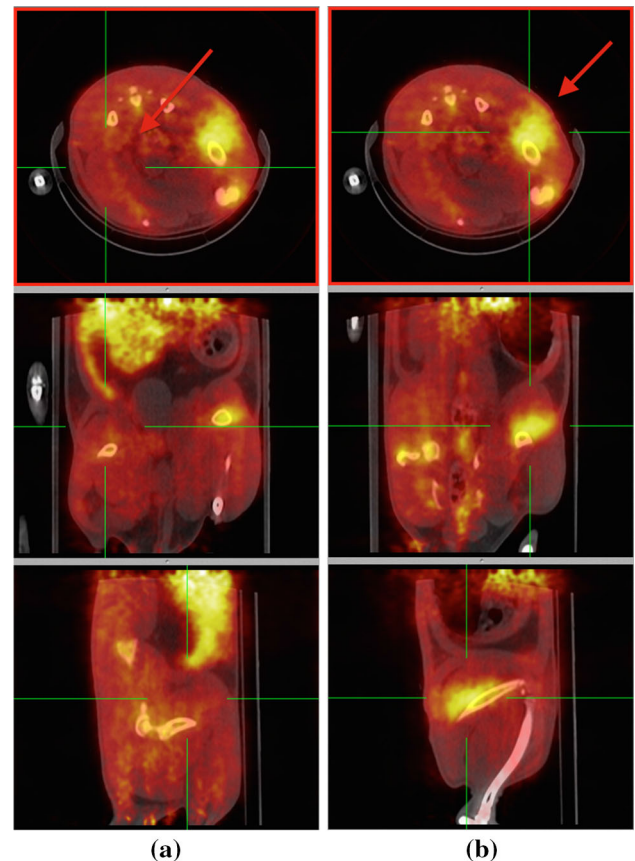


**Fig. 6** Representative fused PET/CT images of the rat hindlimbs after unilateral electrostimulated muscle contractions, showing higher uptake of [ $^{11}\text{C}$ ]acetate in the stimulated *left side* (b), with respect to the inactive *right side* (a)

Kinetic analysis quantitatively confirmed that net tracer uptake ( $K_1$ ) and washout ( $k_2$ ) were significantly higher in exercised muscles ( $K_1 : 0.3 \pm 0.1 \text{ min}^{-1}$  for exercised muscles vs.  $0.18 \pm 0.09 \text{ min}^{-1}$  for resting muscles,  $P = 0.01$ ;  $k_2 : 0.22 \pm 0.05 \text{ min}^{-1}$  for exercised muscle vs.

**Table 2** Net tracer uptake ratio ( $K_1^{Ex}/K_1^{Re}$ ), net tracer washout ratio ( $k_2^{Ex}/k_2^{Re}$ ) and SUV ratio ( $SUV^{Ex}/SUV^{Re}$ ) for the experimental data set

	$K_1^{Ex}/K_1^{Re}$	$k_2^{Ex}/k_2^{Re}$	$SUV^{Ex}/SUV^{Re}$
	1.56	1.35	1.12
	1.47	1.22	1.12
	2.68	1.90	1.28
	2.65	1.96	1.24
	1.54	1.52	1.01
	1.76	1.53	1.21
	2.91	1.81	1.57
	1.38	1.45	0.96
AV	1.99	1.59	1.19
SD	0.64	0.27	0.19

$0.14 \pm 0.04 \text{ min}^{-1}$  for resting muscle,  $P = 0.002$ ). On the other hand, SUV did not result to be significantly different between active and inactive muscles ( $0.7 \pm 0.2$  for exercised muscles vs.  $0.6 \pm 0.1$  for resting muscles) (Fig. 7).

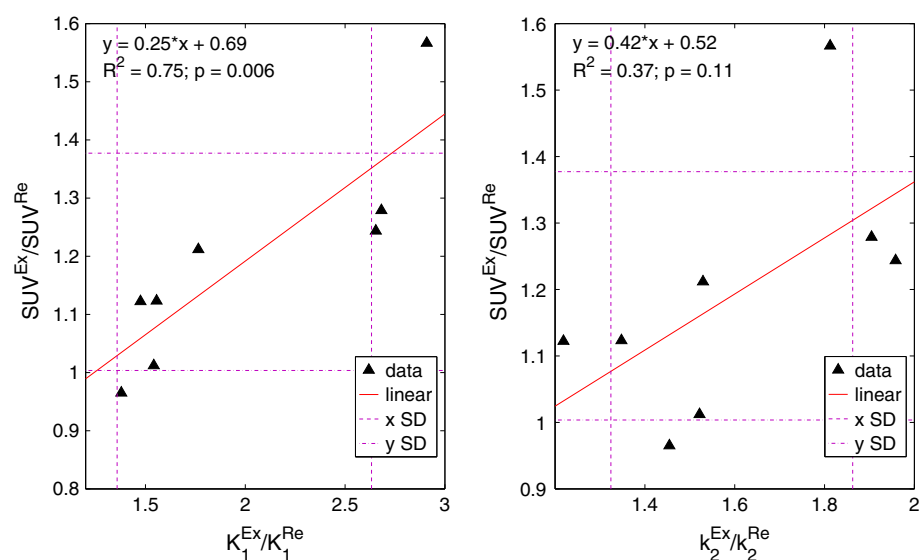
## Discussions and conclusion

The aim of this study was to apply kinetic analysis to investigate exercise-related changes in the metabolism of skeletal muscle of the rat using [ $^{11}\text{C}$ ]acetate PET/CT, and to compare these measures with more conventional SUV measures of tracer uptake in tissue.

Needle electrodes were first applied to rhythmic electrical stimulation of muscles for motor therapy in rats by Kanchiku et al. [23]. In the present study, this technique was applied to induce physiological contractions of the VL muscle within the rat's hindlimb, in order to simulate voluntary repeated

extensions of the knee joint. A significant decrease in joint angular excursion was observed by Jung et al. [22] after a minute of stimulation, and by Kanchiku et al. [23] after 5 min of stimulation, due to muscle fatigue. In our study, a reduction in knee angular excursion was observed after first minutes of stimulation, and in some cases, this decrease led to a complete stop of the movement. Kanchiku et al. [23] did already report the problem of placement of needle electrodes near the motor points of the target muscles. Moreover, not all motor points within the rat's hindlimb are equally easy to reach percutaneously and to stimulate by using needle electrodes. The VL muscle is innervated by the posterior division of the femoral nerve, and the muscle motor point is located under the biceps femoralis and the gluteus superficialis muscles [20]. Therefore, needle electrode placement constituted a delicate phase in our experiment. The complete stops in the electrically induced movement, that occurred during the experiences, were ascribed to the fact that the electrode lost its correct initial placement. Since stimulation sites closer to the motor point require lower charge levels for muscle activation, a misplacement without varying the current amplitude could cause a progressive reduction in the muscular stimulation resulting in a reduced joint angular excursion, eventually up to a complete stop. On the other hand, as previously documented in the literature, we did ascribe the reduced response of the muscle to electrostimulation after electrode repositioning to physiological muscle fatigue. Kanchiku et al. [23], as well as Ichihara et al. [20], reported the possibility to maintain joint angular excursion by incrementally increasing both frequency and current during stimulation. Two variations in the original protocol were investigated in two rats, to test if possible to overcome the problem of electrode repositioning by varying current amplitude and pulse frequency. For our purposes, we considered the exercise induced in the skele-

**Fig. 7** Linear regression analysis revealed a good correlation ( $R^2 = 0.75$ ,  $P = 0.005$ ) between net tracer uptake ratio ( $K_1^{Ex}/K_1^{Re}$ ) and the SUV ratio ( $SUV^{Ex}/SUV^{Re}$ ). A lower correlation was found between the net tracer washout ratio ( $k_2^{Ex}/k_2^{Re}$ ) and the SUV ratio ( $R^2 = 0.37$ ,  $P = 0.1$ )





tal muscle by the three protocols as reasonably uniform to consider our experimental set as homogeneous.

Kinetic analysis methods require the measurement of the radioactivity distribution within the target tissue as well as the extraction of an arterial IF, which describes the radioactivity distribution in the blood. Dynamic PET imaging allows for noninvasive measurement of tissue tracer concentration in time. On the other hand, several different methods can be used to define the IF. An IDIF can be obtained from the dynamic PET images, where a suitably large blood vessel can be located within the PET FOV [9, 12, 27].<sup>1</sup> As an alternative, an external mean can be used for blood sampling. Conventionally, fast sequential manual blood sampling is considered as the gold standard to obtain accurate IF. However, this technique is challenging in small animal experiments due to the small amounts of blood available, and limits the temporal resolution of the measurements. Moreover, the reduction in the blood volume can alter animal's physiology [10], and in many cases, when the peak concentration of tracer in the arterial blood is found within the first seconds after a bolus intravenous injection of the tracer, as for [<sup>11</sup>C]acetate, it can be missed when manual sampling is performed. For all these reasons, arterial blood sampling may be inadequate in accurately capturing the rapid kinetics of the IF. Therefore, alternative methods have been proposed in the literature. These involves hybrid methods, combining image-derived and blood sampling measurement techniques [19, 38, 41], or the use of a standard IF calibrated by a limited number of blood samples [30]. Otherwise, beta microprobe systems [26, 33, 44] and beta microvolumetric blood counter systems [6, 7, 28] have been described. A very good agreement between gold-standard data from manual sampling and from  $\mu$ BC systems was proven in the literature [6, 27]. For all these reasons, in the present study, a microvolumetric flow-through  $\mu$ BC was used for continuous measurement of the arterial radioactivity concentration.

To be used as an IF in a kinetic model, experimental blood activity concentrations must be corrected for several factors. In particular, the injected tracer bolus experiences a dispersion effect, identified in literature as the smearing out due to inhomogeneous velocity fields in the vessels while moving from the injection site to the tissue of interest. In this study, the sampling site was set in the carotid artery, whereas the target tissue was the VL muscle located in the left hindlimb of the rat. Therefore, both dispersion effects of radioactivity moving within the body and through the catheter from the sampling site to the  $\mu$ BC had to be considered. Warnock et al. [44] demonstrated that the shape of an IF measured with a

beta-probe did not vary, in rat studies, whether the shunt arterial source was located in the femoral artery or in the carotid artery. Since dispersion effects affect the shape of the IF and the femoral artery is located within the hindlimb, we considered reasonable to evaluate as negligible the dispersion effect between the carotid artery and the target tissue located within the rat hindlimb. Thus, we assumed that the major dispersion effect was due, in our case, to the presence of the catheter connecting the carotid sampling site to the  $\mu$ BC.

The one-leg knee-extensor exercise model is the most frequently used model in the literature to study active skeletal muscle energy metabolism. This model makes it possible to simultaneously study acetate kinetics and carbon recovery in an active and inactive leg skeletal muscle without differences in hormonal and metabolite concentrations [13]. Our study is conceived as a preclinical step towards the development of a model applicable in humans for in vivo quantitative assessment of muscular activity within a clinical environment. Thus, we considered as appropriate and beneficial the use of a compartment model approach to study the activity rate of [<sup>11</sup>C]acetate within the muscle. In fact, results from model-fitting approach are expected to be more valid over a wider range of physiological conditions. In other words, when the study would be translated to the clinic, the advantages of the model fitting are expected to become more evident [39].<sup>2</sup>

In our study design, a one-tissue compartment model was used to model [<sup>11</sup>C]acetate kinetics within rat's skeletal muscle. The rationale for the modelling approach chosen for this specific tracer was to limit the uncertainty of the parameter estimates, compared to method of higher complexity. Thus, it could be expected that most of the error arises from noisy or bias experimental data [14]. Measurements taken with [<sup>13</sup>C]acetate by van Hall et al. [13] have shown that the average uptake of acetate for the leg muscle at rest is 15  $\mu$ mol min<sup>-1</sup>, with a release rate of 5  $\mu$ mol min<sup>-1</sup>, which accounts for 4 and 1.5 % of the available acetate, respectively. During exercise, the contribution of leg acetate uptake to the whole-body acetate disposal increased sixfold to 25 % and contribution of leg acetate release to the acetate whole-body rate of appearance increased ninefold with 13 %. At rest, the leg blood flow was 30 ml min<sup>-1</sup>. With exercise, the blood flow to the exercising leg increased 13-fold to 3.9 l min<sup>-1</sup>. Blood flow to the resting leg increases 2.5-fold to 0.8 l min<sup>-1</sup>. This indicates that not a complete resting leg is studied as intended. The blood flow to the resting leg is most likely increased due to muscle activity in that leg needed to stabilize the body, while the other leg is exercising. Therefore, a one-tissue compartment model was assumed to be appropriate in our experimental case, where we were

<sup>1</sup> This approach is generally preferred in patients, because of the invasiveness of arterial sampling. However, these methods may offer limited accuracy, require complex correcting factors and lack the necessary temporal resolution.

<sup>2</sup> Moreover, clinically feasible model-fitting algorithm have recently been applied on whole-body dynamic PET human studies [24]

concerned with estimating kinetic parameters from skeletal muscle tissue after exercise, which has high blood flow rates, and the contralateral muscle, where higher blood flow rates were reported, when compared to a complete resting leg as intended.

Results from our study show a higher sensitivity of the kinetic analysis with respect to the SUV in detecting changes between active and inactive skeletal muscles, when performed with [ $^{11}\text{C}$ ]acetate PET/CT. This could be attributed to the capability of dynamic PET imaging and kinetic analysis in taking into account the temporal rate of biological changes between rest and stress condition. This preclinical study in an animal model is ultimately intended as a proof of concept towards the development of a model applicable in humans for in vivo quantitative assessment of muscular activity. Its applicability in a clinical environment could include different practical applications, where the identification of active and nonactive muscles during exercise may have an important role in patient management and follow-up. Among the most relevant applications is muscle recovery after injury or surgery. This would allow more objective evaluation of certain interventional techniques as well as the efficacy of rehabilitation and physiotherapy in patients after surgery.

**Acknowledgments** This work was supported by the European Marie-Curie project Multiscale Biological Modalities for Physiological Human Articulation (MSH - Grant Agreement: 289897), and by the Centre for Biomedical Imaging (CIBM), Geneva, CH. Many thanks are due to Prof. Daniel Huber (Huberlab, Department of Fundamental Neurosciences, University Medical Centre (CMU), Geneva, CH) for kindly providing part of the laboratory equipment.

#### Compliance with ethical standards

**Conflict of interest** Sara Trombella, David García, Didier J. Colin, Stéphane Germain, Yann Seimille and Osman Ratib declare no conflicts of interest.

**Animal ethical standards** All institutional and national guidelines for the care and use of laboratory animals were followed.

## References

- Armbrecht JJ, Buxton DB, Schelbert HR (1990) Validation of [ $^{11}\text{C}$ ]acetate as a tracer for noninvasive assessment of oxidative metabolism with positron emission tomography in normal, ischemic, postischemic, and hyperemic canine myocardium. *Circulation* 81:1594–1605
- Bentourkia M, Croteau T, Langlois R, Aliaga A, Cadorette J, Benard F, Lesur O, Lecomte R (2002) Cardiac studies in rats with  $^{11}\text{C}$ -acetate and PET: a comparison with  $^{13}\text{N}$ -ammonia. *IEEE Trans Nucl Sci* 49:231–238
- Boellaard R, Knaapen P, Rijbroek A, Luurtsema GJJ, Lammertsma AA (2005) Evaluation of basis function and linear least squares methods for generating parametric blood flow images using  $^{15}\text{O}$ -water and positron emission tomography. *Mol Imaging Biol* 7:273–285
- Buchegger F, Ratib O, Willi JP, Steiner C, Seimille Y, Zaidi H, Graf V, Peter R, Jung M (2011) [ $^{11}\text{C}$ ]acetate PET/CT visualizes skeletal muscle exercise participation, impaired function, and recovery after hip arthroplasty: first results. *Mol Imaging Biol* 13:793–799
- Buck A, Wolpers HG, Hutchins GD, Savas V, Mangner TJ, Nguyen N, Schwaiger M (1991) Effect of carbon-11-acetate recirculation on estimates of myocardial oxygen consumption by PET. *J Nucl Med* 32:1950–1957
- Convert L, Morin-Brassard G, Cadorette J, Archambault M, Bentourkia M, Lecomte R (2007) A new tool for molecular imaging: the microvolumetric  $\beta$  blood counter. *J Nucl Med* 48:1197–1206. doi:10.2967/jnumed.107.042606
- Convert L, Morin-Brassard G, Cadorette J, Rouleau D, Croteau E, Archambault M, Fontaine R, Lecomte R (2007) A microvolumetric  $\beta$  blood counter for pharmacokinetic PET studies in small animals. *IEEE Trans Nucl Sci* 54(1):173–180
- Croteau E, Gascon S, Bentourkia M, Langlois R, Rousseau JA, Lecomte R, Bénard F (2012) [ $^{11}\text{C}$ ]acetate rest-stress protocol to assess myocardial perfusion and oxygen consumption reserve in a model of congestive heart failure in rats. *Nucl Med Biol* 39:287–294
- Croteau E, Lavallée E, Labbe SM, Hubert L, Pifferi F, Rousseau JA, Cunnean SC, Carpentier AC, Lecomte R, Bénard F (2010) Image-derived input function in dynamic human PET/CT: methodology and validation with  $^{11}\text{C}$ -acetate and  $^{18}\text{F}$ -fluorothioheptadecanoic acid in muscle and  $^{18}\text{F}$ -fluorodeoxyglucose in brain. *Eur J Nucl Med Mol Imaging* 37:1539–1550. doi:10.1007/s00259-010-1443-z
- Diehl KH, Hull R, Morton D, Pfister R, Rabemampianina Y, Smith D, Vidal JM, van de Vortebosch C (2001) A good practice guide to the administration of substances and removal of blood, including routes and volumes. *J Appl Toxicol* 21:15–23
- Feng D, Wang Z, Huang S (1993) A study on statistically reliable and computationally efficient algorithms for generating local cerebral blood-flow parametric images with positron emission tomography. *IEEE Trans Med Imaging* 12:182–188
- Germano G, Chen BJ, Huang SC, Gambhir SS, Hoffman EJ, Phelps ME (1992) Use of the abdominal aorta for arterial input function determination in hepatic and renal PET studies. *J Nucl Med* 33(6):613–620
- van Hall G, Sacchetti M, Rådegran G (2002) Whole body and leg acetate kinetics at rest, during exercise and recovery in humans. *J Physiol* 542(1):263–272. doi:10.1113/jphysiol.2001.014340
- Herrero P, Kim J, Sharp TL, Engelbach JA, Lewis JS, Gropler RJ, Welch MJ (2006) Assessment of myocardial blood flow using  $^{15}\text{O}$ -water and  $^{11}\text{C}$ -acetate in rats with small-animal PET. *J Nucl Med* 47:477–485
- van den Hoff J, Burchert W, Börner AR, Fricke H, Kühnel G, Meyer GJ, Otto D, Weckesser E, Wolpers HG, Knapp WH (2001) [ $^{11}\text{C}$ ]acetate as a quantitative perfusion tracer in myocardial PET. *J Nucl Med* 42:1174–1182
- van den Hoff J, Burchert W, Müller-Schauenburg W, Meyer GJ, Hundeshagen H (1993) Accurate local blood flow measurements with dynamic PET: fast determination of input function delay and dispersion by multilinear minimization. *J Nucl Med* 34:1770–1777
- van den Hoff J, Burchert W, Wolpers HG, Meyer GJ, Hundeshagen H (1996) A kinetic model for cardiac PET with [ $^{11}\text{C}$ ]acetate. *J Nucl Med* 37:521–529
- Huang SC (2000) Anatomy of SUV. *Nucl Med Biol* 27:643–646
- Huang SC, Wu HM, Shoghi-Jadid K, Stout DB, Chatziioannou A, Schelbert HR, Barrio JR (2004) Investigation of a new input function validation approach for dynamic mouse microPET studies. *Mol Imaging Biol* 6(1):34–46. doi:10.1016/j.mibio.2003.12.002
- Ichihara K, Venkatasubramanian G, Abbas JJ, Jung R (2009) Neuromuscular electrical stimulation of the hindlimb muscles for movement therapy in a rodent model. *J Neurosci Methods* 176:213–224

21. Iida H, Kanno I, Miura S, Murakami M, Takahashi K, Uemura K (1986) Error analysis of a quantitative cerebral blood flow measurement using  $H_2^{15}O$  autoradiography and positron emission tomography, with respect to the dispersion of the input function. *J Cereb Blood Flow Metab* 6:536–545
22. Jung R, Belanger A, Kanchiku T, Fairchild M, Abbas JJ (2009) Neuromuscular stimulation therapy after incomplete spinal cord injury promotes recovery of interlimb coordination during locomotion. *J Neural Eng* 6(055010):1–14. doi:[10.1088/1741-2560/6/5/055010](https://doi.org/10.1088/1741-2560/6/5/055010)
23. Kanchiku T, Kato Y, Suzuki H, Imajo Y, Yoshida Y, Moriya A, Taguchi T, Jung R (2012) Development of less invasive neuromuscular electrical stimulation model for motor therapy in rodents. *J Spinal Cord Med* 35(3):162–169. doi:[10.1179/2045772312Y.0000000009](https://doi.org/10.1179/2045772312Y.0000000009)
24. Karakatsanis NA et al (2013) Dynamic whole-body PET parametric imaging: I. Concept, acquisition protocol optimization and clinical application. *Phys Med Biol* 58:7391–7418
25. Kotzerke J, Volkmer BG, Neumaier B, Gschwend JE, Hautmann RE, Reske SN (2002) Carbon-11 acetate positron emission tomography can detect local recurrence of prostate cancer. *Eur J Nucl Med Mol Imaging* 29(10):1380–1384
26. Laforest R, Sharp TL, Engelbach JA (2005) Measurement of input functions in rodents: challenges and solutions. *Nucl Med Biol* 32:679–685
27. Lanz B, Poitry-Yamate C, Gruetter R (2014) Image-derived input function from the Vena Cava for 18F-FDG PET studies in rats and mice. *J Nucl Med* 55:1–9
28. Lapointe D, Cadorette J, Rodrigue S, Rouleau D, Lecomte R (1998) A microvolumetric blood counter/sampler for metabolic PET studies in small animals. *IEEE Trans Nucl Sci* 45(4):2195–2199
29. Magnenat-Thalmann N, Ratib O, Choi HF (2014) 3D multiscale physiological human. Springer, Berlin
30. Meyer PT, Circiumaru V, Cardi CA, Thomas DH, Bal H, Acton PD (2006) Simplified quantification of small animal [18F]FDG PET studies using a standard arterial input function. *Eur J Nucl Med Mol Imaging* 33:948–954
31. Ng CK, Huang SC, Schelbert HR, Buxton DB (1994) Validation of a model for [1-11C]acetate as a tracer of cardiac oxidative metabolism. *Am J Physiol* 266:H1304–H1315
32. Oyama N, Akino H, Kanamaru H, Suzuki Y, Muramoto S, Yonekura Y, Sadato N, Yamamoto K, Okada K (2002) 11C-acetate PET imaging of prostate cancer. *J Nucl Med* 43(2):181–186
33. Pain F, Lanière P, Mastrippolito R, Gervais P, Hantraye P, Besret L (2004) Arterial input function measurement without blood sampling using a  $\beta$ -microprobe in rats. *J Nucl Med* 45:1577–1582
34. Peckham PH, Knutson JS (2005) Functional electrical stimulation for neuromuscular applications. *Annu Rev Biomed Eng* 7:327–360. doi:[10.1146/annurev.bioeng.6.040803.140103](https://doi.org/10.1146/annurev.bioeng.6.040803.140103)
35. Prasad R, Ratib O, Zaidi H (2010) Performance evaluation of the FLEX Triumph X-PET scanner using the National Electrical Manufacturers Association NU-4 standards. *J Nucl Med* 51:1608–1615. doi:[10.2967/jnumed.110.076125](https://doi.org/10.2967/jnumed.110.076125)
36. Rosset A, Spadola L, Ratib O (2004) Osirix: an open-source software for navigating in multidimensional dicom images. *J Digit Imaging* 17(3):205–216
37. Schiepers C, Hoh CK, Nuyts J, Seltzer M, Wu C, Huang SC, Dahlbom M (2008) 1-11C-acetate kinetics of prostate cancer. *J Nucl Med* 49:206–215. doi:[10.2967/jnumed.107.044453](https://doi.org/10.2967/jnumed.107.044453)
38. Shoghi KI, Welch MJ (2007) Hybrid image and blood sampling input function for quantification of small animal dynamic PET data. *Nucl Med Biol* 34:989–994
39. Sun KT, Chen K, Huang SC, Buxton DB, Hansen HW, Kim AS, Siegel S, Choi Y, Muller P, Phelps ME, Scheiben HR (1997) Compartment model for measuring myocardial oxygen consumption using [1-11C]acetate. *J Nucl Med* 38:459–466
40. Sun KT, Yeatman LA, Buxton DB, Chen K, Johnson JA, Huang SC, Kofoed KF, Weismueller S, Czernin J, Phelps ME, Schelbert HR (1998) Simultaneous measurement of myocardial oxygen consumption and blood flow using [1-carbon-11]acetate. *J Nucl Med* 39:272–280
41. Tantawy MN, Peterson TE (2010) Simplified [18F]FDG image-derived input function using the left ventricle, liver, and one venous blood sample. *Mol Imaging* 9(2):76–86
42. Thota AK, Watson SC, Knapp E, Thompson B, Jung R (2005) Neuromechanical control of locomotion in the rat. *J Neurotrauma* 25(4):442–465
43. Vavere AL, Kridel SJ, Wheeler FB, Lewis JS (2008) 1-11C-acetate as a PET radiopharmaceutical for imaging fatty acid synthase expression in prostate cancer. *J Nucl Med* 49(2):327–334
44. Warnock G, Bahri MA, Goblet D, Giacomelli F, Lemaire C, Aerts J, Seret A, Langlois X, Luxen A, Plenevaux A (2011) Use of a beta microprobe system to measure arterial input function in PET via arteriovenous shunt in rats. *EJNMMI Res* 1:13